

Intermediate and Power-Law Inflation in the Tachyon Model with Constant Sound Speed

Narges Rashidi^{a,b, 1}

^(a)Department of Theoretical Physics, Faculty of Science, University of Mazandaran,
P. O. Box 47416-95447, Babolsar, IRAN

^(b) ICRA.Net-Mazandaran, University of Mazandaran,
P. O. Box 47416-95447, Babolsar, IRAN

Abstract

By adopting the intermediate and power-law scale factors, we study the tachyon inflation with constant sound speed. We perform some numerical analysis on the perturbation and non-gaussianity parameters in this model and compare the results with observational data. By using the constraints on the scalar spectral index and tensor-to-scalar-ratio, obtained from Planck2018 TT, TE, EE+lowE+lensing+BAO+BK14 data, the constraint on the running of the scalar spectral index obtained from Planck2018 TT, TE, EE+lowEB+lensing data, and constraint on tensor spectral index obtained from Planck2018 TT, TE, EE +lowE+lensing+BK14+BAO+LIGO and Virgo2016 data, we find the observationally viable ranges of the model's parameters at both 68% CL and 95% CL. We also analyze the non-gaussian features of the model in the equilateral and orthogonal configurations. Based on Planck2018 TTT, EEE, TTE and EET data, we find the constraints on the sound speed as $0.276 \leq c_s \leq 1$ at 68% CL, $0.213 \leq c_s \leq 1$ at 95% CL, and $0.186 \leq c_s \leq 1$ at 97% CL.

1 Introduction

Considering that the early time inflation in the history of the universe seems to have occurred around Planck's scale, the M/String theory inspired fields can be a possible candidate for the field responsible for inflation. Tachyon inflation is one of these fields leading to interesting cosmological results. Tachyon field, which has attained a lot of attention, is associated with the D-branes in string theory. One interesting implication of this field is that, its slow-rolling down to the potential leads to the smooth evolution of the universe from the accelerating phase of the expansion to the era dominated by the non-relativistic fluid [44, 45, 46, 19].

On the other hand, we know that in the simple inflation model with canonical scalar fields, we find the primordial perturbation to be scale-invariant and gaussian [20, 27, 5, 28, 25, 26, 42, 29, 30]. When we consider an inflation model with a canonical scalar field, we find a gaussian perturbation that the values of its tensor-to-scalar ratio for ϕ , ϕ^2 , $\phi^{4/3}$ are not consistent with observational data [3]. Therefore we have to seek some other specific potential like hilltop potential to get an observationally viable single canonical field inflation model [3]. However, with every potential, the amplitude of the primordial perturbation in the single canonical field inflation is almost gaussian. Or, we should consider a nonminimal inflation model to give a better explanation of the early time cosmological inflation. However, with a non-canonical scalar field like tachyon,

¹n.rashidi@umz.ac.ir

it is possible to get the scale-dependent and non-gaussian distribution for the amplitude of the primordial perturbations. Another interesting point about the tachyon field is corresponding to the equation of state of the tachyon field. This parameter in the tachyon field can be -1 , which describes both very early time and very late time accelerating expansion of the universe. Also, its value can be 0, describing the matter/dark matter dominated era. Therefore, with the tachyon field it is possible to explain the thermal history of the universe in a reasonable way [19]. These are interesting issues that motivate cosmologists to consider and study the inflation models driven by a tachyon field as a non-canonical scalar field. In this regard, a lot of interesting works based on tachyon inflation have been done. For instance, the authors of Ref. [23] have considered a tachyon field in the context of quantum loop gravity. In this way, they have obtained the inflation and perturbation parameters and tested the observational viability of some inflation models. In ref. [12], by considering the holographic cosmology, the tachyon inflation has been studied and the results have been compared to the observational data. The authors of Ref. [31] have studied an inflation model where a tachyon field interacts with photon gas. They have shown that under some assumptions and conditions this model shows some agreement with observational data. In [38], the tachyon model with a superpotential, a potential based on supersymmetry, has been studied. It has been shown that tachyon inflation with a superpotential, at least in some ranges of the model's parameter space, is consistent with observational data. There are other works on tachyon inflation leading to interesting cosmological results [32, 36, 13, 41, 39, 40] and all of these works show that the tachyon field can be considered as a field running the inflation.

One of the important parameters in the inflation models is the sound speed of the primordial perturbation, shown by c_s . The sound speed is corresponding to the Lorentz factor γ as $c_s = \frac{1}{\gamma}$. For the canonical scalar field, we get the sound speed equal to unity. However, with the non-canonical scalar fields, we have $c_s^2 \neq 1$. The value of the parameter γ and correspondingly sound speed determines the deformation of the field's kinetic energy from the canonical one. The constant sound speed is an interesting idea motivated by the authors in Refs. [47, 48]. Considering that in the non-canonical scalar field the sound speed is related to the time variation of the field, the constant sound speed is corresponding to the constant field's variation in times. This can lead to interesting results. Now, the question is what constant values of c_s we should adopt, to study the model numerically. Considering that the sound speed is related to the amplitude of the non-gaussianity, by using the observational constraints on the amplitude of the non-gaussianity, we can find suitable ranges of the sound speed. Also, there are some other parameters, such as the scalar spectral index, tensor spectral index, and tensor-to-scalar ratio that help us to find some constraints on the sound speed values.

To perform a numerical analysis, we use the Planck2018 constraints on the inflation parameters. Based on the Λ CDM + r + $\frac{dn_s}{d \ln k}$ model, the Planck2018 TT, TE, EE+lowE+lensing+BAO+BK14 data gives the value of the scalar spectral index as $n_s = 0.9658 \pm 0.0038$ and implies a constraint on the tensor-to-scalar ratio as $r < 0.072$ [2, 3]. The constraint on the tensor spectral index, released by Planck2018 TT, TE, EE +lowE+lensing+BK14+BAO+LIGO and Virgo2016 data is $-0.62 < n_T < 0.53$ [2, 3]. Also, from Planck2018 TT, TE, EE+lowEB+lensing data, we have the value of the running of the scalar spectral index as $\alpha_s = -0.0085 \pm 0.0073$ [2, 3]. Other useful constraints are corresponding to the amplitude of the non-gaussianity. The planck2018 combined temperature and polarization analysis gives the constraints on the amplitude of the non-gaussianity in the equilateral configuration as $f_{NL}^{equil} = -26 \pm 47$ and in the orthogonal configuration as $f_{NL}^{ortho} = -38 \pm 24$ [4]. These several constraints determine the observational viability of every

inflation model.

With these preliminaries, this paper is organized as follows. In section 2, we review the inflation in a tachyon model with constant sound speed. In this section, we present the main equations governing the dynamics of the model in terms of the sound speed. In section 3, we consider an intermediate scale factor and study the perturbation and non-gaussianity parameters in this model numerically. We compare the results with several data sets to find some constraints on the model's parameter space. In section 4 we study the power-law tachyon inflation with constant sound speed and compare the results with observational data. In section 5, we perform some discussion on unifying the initial inflation with late time dark energy in the tachyon model with constant sound speed. In section 6, we present a summary of this work.

2 Review on the Tachyon Inflation with Constant Sound Speed

For the tachyon field, we have the following Dirac-Born-Infeld type effective 4-dimensional action

$$S = \int d^4x \sqrt{-g} \left[\frac{1}{2\kappa^4} R - V(\phi) \sqrt{1 - 2X} \right], \quad (1)$$

with κ being the gravitational constant, R as the Ricci scalar, and $X = -\frac{1}{2} \partial_\mu \phi \partial^\mu \phi$. Also, the tachyon field ϕ has the potential $V(\phi)$. Cosmologists believe that the physics of the tachyon condensation can be described by such an action. Einstein's field equations, corresponding to action (1), are given by

$$G_{\mu\nu} = \kappa^2 \left[-g_{\mu\nu} V(\phi) \sqrt{1 - 2X} + \frac{V(\phi) \partial_\mu \phi \partial_\nu \phi}{\sqrt{1 - 2X}} \right], \quad (2)$$

which have been obtained by varying action (1) with respect to the metric. Considering the FRW metric as

$$ds^2 = -dt^2 + a^2(t) \delta_{ij} dx^i dx^j, \quad (3)$$

we find the following Friedmann equation

$$3H^2 = \frac{\kappa^2 V(\phi)}{\sqrt{1 - \dot{\phi}^2}}. \quad (4)$$

corresponding to the (0,0) component of Einstein's field equations. Note that, a dot on the parameter shows the derivative of the parameter with respect to the time. Also, the (i,i) component of Einstein's field equations give the following second Friedmann equation

$$2\dot{H} + 3H^2 = \kappa^2 \left[V(\phi) \sqrt{1 - \dot{\phi}^2} \right]. \quad (5)$$

We find the equation of motion of the tachyon field by varying the action (1) with respect to the field as

$$\frac{\ddot{\phi}}{1 - \dot{\phi}^2} + 3H\dot{\phi} + \frac{V'(\phi)}{V(\phi)} = 0, \quad (6)$$

where a prime shows the derivative with respect to the tachyon field. Since our purpose in this paper is to study the tachyon model with constant sound speed, we should re-write the above main equations in terms of the sound speed. To this end, we need to define the sound speed of the tachyon field. In general, the square of the sound speed is given by $c_s^2 \equiv \frac{P_{,X}}{\rho_{,X}}$, that in the tachyon model takes the following form

$$c_s = \sqrt{1 - \dot{\phi}^2}. \quad (7)$$

In this regard, the equations (4)-(6) take the following forms

$$3H^2 = \frac{\kappa^2 V(\phi)}{c_s}, \quad (8)$$

$$2\dot{H} + 3H^2 = \kappa^2 V(\phi) c_s, \quad (9)$$

and

$$3H \sqrt{1 - c_s^2} + \frac{V'(\phi)}{V(\phi)} = 0, \quad (10)$$

where we have considered the sound speed as a constant parameter. To study cosmological inflation, we need the following slow-roll parameters

$$\epsilon = -\frac{\dot{H}}{H^2}, \quad (11)$$

$$\eta = -\frac{1}{H} \frac{\ddot{H}}{\dot{H}}. \quad (12)$$

Note that, in the case of the constant sound speed, the third slow-roll parameter $s = \frac{1}{H} \frac{\dot{c}_s}{c_s}$ is zero. Another needed parameter to study inflation is the number of e-folds parameter defined as

$$N = \int H dt. \quad (13)$$

These parameters are useful to study the primordial perturbations in the model and compare the results with observational data. The observational data that we use in our work is the data released by the Planck2018 team [2, 3, 4]. Based on the fact that, under the assumption of statistical isotropy, the two-point correlations of the CMB anisotropies are described by the angular power spectra C_l^{TT} , C_l^{TE} , C_l^{EE} , and C_l^{BB} (where the subscript l shows the multipole moment number) [24, 49, 43, 22, 21], the Planck team has obtained some constraints on the important perturbation parameters. To include the contributions from the scalar and tensor perturbations in the CMB angular power spectra, the Planck team has used the following expressions [1]

$$C_l^{ab,s} = \int_0^\infty \frac{dk}{k} \Delta_{l,a}^s(k) \Delta_{l,b}^s(k) \mathcal{A}_s(k), \quad (14)$$

$$C_l^{ab,T} = \int_0^\infty \frac{dk}{k} \Delta_{l,a}^T(k) \Delta_{l,b}^T(k) \mathcal{A}_T(k). \quad (15)$$

In equations (14) and (15), we have shown the transfer functions by $\Delta_{l,a}^s(k)$ and $\Delta_{l,a}^T(k)$. The parameter a and b are given as $a, b = T, E, B$. Also, the primordial power spectrum, the parameter identified by the physics of the primordial universe [1], is shown by $\mathcal{A}_i(k)$ (where, $i = s, T$). Model-independent forms of the scalar and tensor power spectra are given by

$$\mathcal{A}_s(k) = A_s \left(\frac{k}{k_*} \right)^{n_s - 1 + \frac{1}{2} \frac{dn_s}{d \ln k} \ln \left(\frac{k}{k_*} \right) + \frac{1}{6} \frac{d^2 n_s}{d \ln k^2} \ln \left(\frac{k}{k_*} \right)^2 + \dots}, \quad (16)$$

$$\mathcal{A}_T(k) = A_T \left(\frac{k}{k_*} \right)^{n_T + \frac{1}{2} \frac{dn_T}{d \ln k} \ln \left(\frac{k}{k_*} \right) + \dots}. \quad (17)$$

These forms of the scalar and tensor power spectra have been used by the Planck team to compare the perturbation parameters with data. Note that, in equations (16) and (17), A_j shows the scalar (corresponding to $j = s$) and tensor (corresponding to $j = T$) perturbations. Also, the running of the scalar or tensor spectral index and the running of the running of the scalar spectral index are given by $\frac{dn_i}{d \ln k}$ and $\frac{d^2 n_s}{d \ln k^2}$, respectively. One can also find the tensor-to-scalar ratio by using the power spectra as

$$r = \frac{\mathcal{A}_T(k_*)}{\mathcal{A}_s(k_*)}, \quad (18)$$

which is a very important parameter in studying the inflation models. The parameters n_s and n_T are the scalar and tensor spectral indices showing the scale dependence of the primordial perturbations. The scalar spectral index, at the time of sound horizon exit of the physical scales, is defined as

$$n_s - 1 = \left. \frac{d \ln \mathcal{A}_s}{d \ln k} \right|_{c_s k = aH}, \quad (19)$$

where the parameter \mathcal{A}_s , the amplitude of the scalar spectral index, is given by the following definition

$$\mathcal{A}_s = \frac{H^2}{8\pi^2 \mathcal{W}_s c_s^3}, \quad (20)$$

with

$$\mathcal{W}_s = \frac{V(1 - c_s^2)}{2H^2 c_s^3}. \quad (21)$$

The scalar spectral index, in terms of the slow-roll parameters, is written as

$$n_s = 1 - 6\epsilon + 2\eta. \quad (22)$$

This is one of the parameters that can be compared with observational data. Another important parameter in studying the inflation models is the running of the scalar spectral index, defined as

$$\alpha_s = \frac{dn_s}{d \ln k} = 8\epsilon\eta - 12\epsilon^2 - 2\zeta + 2\eta^2, \quad (23)$$

where, the parameter ζ is given by

$$\zeta = \frac{\ddot{H}}{H^2 \dot{H}}. \quad (24)$$

The tensor spectral index, obtained from equation (17), is defined as follows

$$n_T = \left. \frac{d \ln \mathcal{A}_T}{d \ln k} \right|_{k=aH}, \quad (25)$$

with

$$\mathcal{A}_T = \frac{2\kappa^2 H^2}{\pi^2}, \quad (26)$$

being the amplitude of the tensor perturbations. In terms of the slow-roll parameters, the tensor spectral index is expressed as

$$n_T = -2\epsilon. \quad (27)$$

Finally, we have the following expression for the tensor-to-scalar ratio

$$r = 16 c_s \epsilon. \quad (28)$$

As we see in equation (28), the tensor-to-scalar ratio depends explicitly on the sound speed of the perturbations. Therefore, from the observationally viable value of r , we can constrain the values of the sound speed.

Another important parameter that depends on the sound speed parameter is the nonlinearity parameter. The nonlinearity parameter demonstrates the non-gaussian property of the amplitude of the primordial perturbation. The Gaussian distributed primordial perturbations are characterized by a two-point correlation. To seek the additional statistical information, corresponding to the non-Gaussian distributed perturbation, it is necessary to consider the higher-order correlations. The three-point correlation function for the spatial curvature perturbation in the interaction picture is given by [30]

$$\langle \Phi(\mathbf{k}_1) \Phi(\mathbf{k}_2) \Phi(\mathbf{k}_3) \rangle = (2\pi)^3 \delta^3(\mathbf{k}_1 + \mathbf{k}_2 + \mathbf{k}_3) \mathcal{B}_\Phi(\mathbf{k}_1, \mathbf{k}_2, \mathbf{k}_3), \quad (29)$$

with the following definition for the parameter \mathcal{B}_Φ

$$\mathcal{B}_\Phi(\mathbf{k}_1, \mathbf{k}_2, \mathbf{k}_3) = \frac{(2\pi)^4 \mathcal{A}_s^2}{\prod_{i=1}^3 k_i^3} \mathcal{D}_\Phi(\mathbf{k}_1, \mathbf{k}_2, \mathbf{k}_3). \quad (30)$$

The parameter \mathcal{D}_Φ in equation (40) is expressed as follows

$$\mathcal{D}_\Phi = \left(1 - \frac{1}{c_s^2} \right) \left[\frac{3}{4} \mathcal{J}_1 - \frac{3}{2} \mathcal{J}_2 - \frac{1}{4} \mathcal{J}_3 \right], \quad (31)$$

where

$$\mathcal{J}_1 = \frac{2 \sum_{i>j} k_i^2 k_j^2}{k_1 + k_2 + k_3} - \frac{\sum_{i \neq j} k_i^2 k_j^3}{(k_1 + k_2 + k_3)^2}, \quad (32)$$

$$\mathcal{J}_2 = \frac{(k_1 k_2 k_3)^2}{(k_1 + k_2 + k_3)^3}, \quad (33)$$

and

$$\mathcal{J}_3 = \frac{2 \sum_{i>j} k_i^2 k_j^2}{k_1 + k_2 + k_3} - \frac{\sum_{i \neq j} k_i^2 k_j^3}{(k_1 + k_2 + k_3)^2} + \frac{1}{2} \sum_i k_i^3. \quad (34)$$

By using the parameter \mathcal{D}_Φ , one can find the non-linear parameter as

$$f_{NL} = \frac{10}{3} \frac{\mathcal{D}_\Phi}{\sum_{i=1}^3 k_i^3}. \quad (35)$$

Note that, in equation (35), there is a parameter k_i which is the momentum. Depending on different values of the momenta (k_1 , k_2 , and k_3), we get different shapes of the non-gaussianity. In every shape, there is a maximal peak in the amplitude of the perturbations that defines the kind of the corresponding shape. We are interested in the case with a peak at $k_1 = k_2 = k_3$ limit, leading to an equilateral shape, and the case orthogonal to it [15, 6, 17, 11]. It is possible to write the bispectrum (31) in terms of the equilateral and orthogonal shapes basis as follows [17]

$$\mathcal{D}_\Phi = \mathcal{M}_1 \check{\mathcal{J}}^{equil} + \mathcal{M}_2 \check{\mathcal{J}}^{ortho}, \quad (36)$$

where,

$$\check{\mathcal{J}}^{equil} = -\frac{12}{13} (3\mathcal{J}_1 - \mathcal{J}_2). \quad (37)$$

$$\check{\mathcal{J}}^{ortho} = \frac{12}{14 - 13\mathcal{C}} (\mathcal{C}(3\mathcal{J}_1 - \mathcal{J}_2) + 3\mathcal{J}_1 - \mathcal{J}_2), \quad (38)$$

$$\mathcal{M}_1 = \frac{13}{12} \left[\frac{1}{24} \left(1 - \frac{1}{c_s^2} \right) \left(2 + 3\mathcal{C} \right) \right], \quad (39)$$

and

$$\mathcal{M}_2 = \frac{14 - 13\mathcal{C}}{12} \left[\frac{1}{8} \left(1 - \frac{1}{c_s^2} \right) \right], \quad (40)$$

with $\mathcal{C} \simeq 1.1967996$. To see more details to obtain the non-linear parameter, see Refs. [17, 18, 14]. Now, we find the amplitudes of the non-Gaussianity in the equilateral and orthogonal configurations as

$$f_{NL}^{equil} = \frac{130}{36 \sum_{i=1}^3 k_i^3} \left[\frac{1}{24} \left(1 - \frac{1}{c_s^2} \right) \left(2 + 3\mathcal{C} \right) \right] \check{\zeta}^{equil}, \quad (41)$$

and

$$f_{NL}^{ortho} = \frac{140 - 130\mathcal{C}}{36 \sum_{i=1}^3 k_i^3} \left[\frac{1}{8} \left(1 - \frac{1}{c_s^2} \right) \right] \check{\zeta}^{ortho}. \quad (42)$$

The equations (41) and (42) in the $k_1 = k_2 = k_3$ limit become

$$f_{NL}^{equil} = \frac{325}{18} \left[\frac{1}{24} \left(\frac{1}{c_s^2} - 1 \right) \left(2 + 3\mathcal{C} \right) \right], \quad (43)$$

and

$$f_{NL}^{ortho} = \frac{10}{9} \left(\frac{65}{4} \mathcal{C} + \frac{7}{6} \right) \left[\frac{1}{8} \left(1 - \frac{1}{c_s^2} \right) \right]. \quad (44)$$

Up to this point, we have presented the main equations describing the cosmological dynamics of the tachyon model. In the following, we adopt two types of scale factor (power-law and intermediate) for the tachyon model with constant sound speed and study its observational viability.

3 Intermediate Tachyon Inflation with Constant-Sound Speed

In this section, we study the intermediate inflation in the tachyon model with constant sound speed. In the intermediate inflation, we have the following scale factor [8, 9, 10]

$$a = a_0 \exp \left(b t^\beta \right), \quad (45)$$

where, $0 < \beta < 1$ and b is a constant. This scale factor demonstrates that in this case, the expansion of the universe is slower than an exponential expansion and faster than a power-law expansion. From the intermediate scale factor (41) we find the Hubble parameter as

$$H(N) = N \left(\frac{N}{b} \right)^{-\frac{1}{\beta}} \beta. \quad (46)$$

To use this Hubble parameter and study the observational viability of the model, we need to reconstruct the potential and the inflation parameters in terms of the Hubble parameter and its derivatives [7, 37]. From equation (8) we obtain the potential as

$$V = 3 \frac{H^2(N) c_s}{\kappa^2}. \quad (47)$$

Also, the slow-roll parameters take the following form

$$\epsilon = - \frac{\frac{d}{dN} H(N)}{H(N)}, \quad (48)$$

and

$$\eta = \frac{\left(\left(\frac{d}{dN} H(N) \right)^2 \sqrt{1 - c_s^2} + (c_s - 1)(c_s + 1) \left(H(N) \frac{d^2}{dN^2} H(N) + 2 \left(\frac{d}{dN} H(N) \right)^2 \right) \right)}{\sqrt{1 - c_s^2} H(N) \frac{d}{dN} H(N)}. \quad (49)$$

By using the above equations, we can rewrite equations (22), (23), (27) and (28), in terms of the Hubble parameter and its derivatives. After that, by using equation (46), we can obtain the scalar spectral index, its running, tensor spectral index, and tensor-to-scalar ratio in terms of the intermediate parameters and also the sound speed. Then we perform some numerical analysis and, to obtain some constraints on the model's parameters, we compare the results with observational data. The results have been shown in several figures. Figure 1 shows the tensor-to-scalar ratio of the intermediate tachyon model with constant sound speed versus the scalar spectral index in

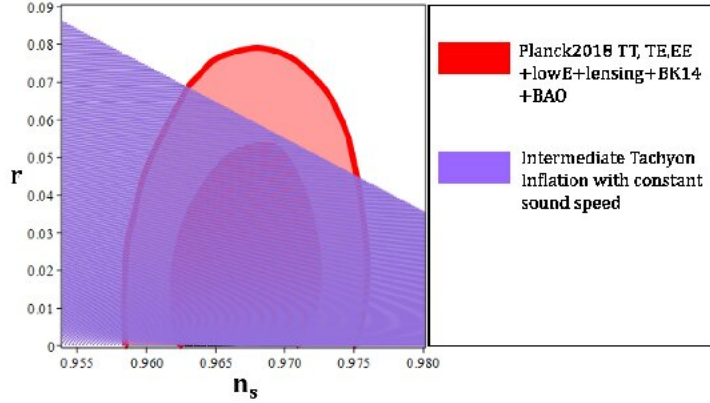


Figure 1: Tensor-to-scalar ratio versus the scalar spectral index in the intermediate tachyon model with constant sound speed.

this model, in the background of the Planck2018 TT, TE, EE+lowE+lensing+BAO+BK14 data at 68% CL and 95% CL. As we can see from figure 1, this model in some ranges of the model's parameter space is consistent with observational data. Our numerical analysis shows that the intermediate tachyon model with constant sound speed is consistent with Planck2018 TT, TE, EE+lowE+lensing+BAO+BK14 data at 95% CL, if $0 < c_s \leq 1$ and $0.787 \leq \beta \leq 1$. Also, this model is consistent with Planck2018 TT, TE, EE+lowE+lensing+BAO+BK14 data at 68% CL, if $0 < c_s \leq 0.997$ and $0.833 \leq \beta \leq 1$. Figure 2 shows the running of the scalar spectral index of the intermediate tachyon model with constant sound speed versus the scalar spectral index in this model, in the background of the Planck2018 TT, TE, EE+lowE+lensing data at 68% CL and 95% CL. By studying these parameters, we find that $\alpha_s - n_s$ of the intermediate tachyon model with constant sound speed is consistent with Planck2018 TT, TE, EE+lowE+lensing data at 68% CL, if $0 < c_s \leq 1$ and $0.756 \leq \beta \leq 1$ and at 95% CL, if $0 < c_s \leq 1$ and $0.812 \leq \beta \leq 1$. The evolution of the tensor-to-scalar ratio of the intermediate tachyon model with constant sound speed versus the tensor spectral index in this model, in the background of the Planck2018 TT, TE, EE+lowE+lensing+BK14 +BAO+LIGO and Virgo2016 data at 68% CL and 95% CL, has been shown in figure 3. The obtained constraints in this case are $0 < c_s \leq 1$ and $0.081 \leq \beta \leq 0.984$ at 68% CL and $0 < c_s \leq 1$ and $0.027 \leq \beta \leq 1$ at 95% CL.

We have also performed some numerical analysis to find the domain of β and c_s , leading to observationally viable values of scalar spectral index, tensor spectral index, and tensor-to-scalar ratio. The results are shown in figure 4, where we have used both Planck2018 TT, TE, EE+lowE+lensing+BAO+BK14 and Planck2018 TT, TE, EE+lowE+lensing+BK14 +BAO+LIGO and Virgo2016 data sets at 68% CL and 95% CL. Both panels confirm that, depending on the value of sound speed, the observationally viable values of β start from almost 0.75. The interesting point is that for these ranges of parameter space, the amplitude of the scalar perturbation is consistent with observational data too. The constraint on the amplitude of the scalar perturbation, obtained from Planck2018 TT, TE, EE+lowE+lensing data, is $\ln(10^{10} A_s) = 3.044 \pm 0.014$. By this observational constraint, we have obtained the observational viable domain of c_s and β , shown in figure 5. Another way to check the observational viability of the model is to study the amplitudes of the non-gaussianity nu-

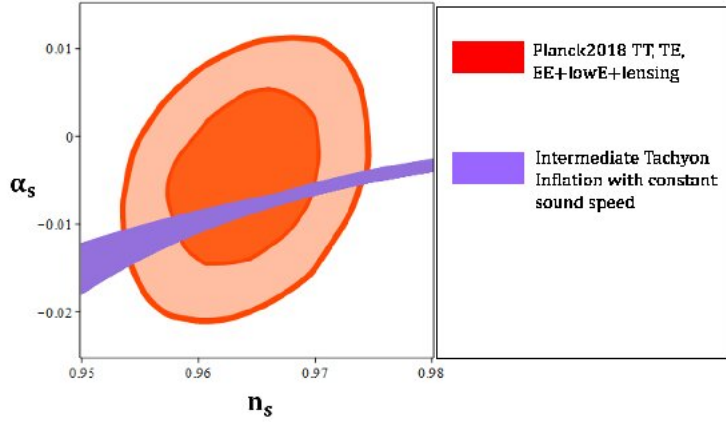


Figure 2: Running of the scalar spectral index versus the scalar spectral index in the intermediate tachyon model with constant sound speed.

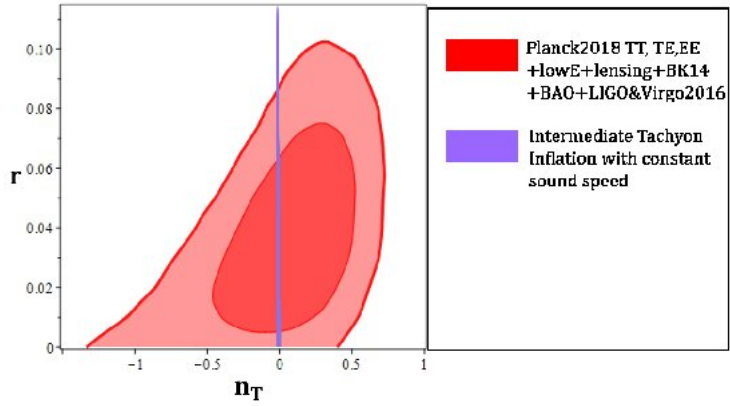


Figure 3: Tensor-to-scalar ratio versus the tensor spectral index in the intermediate tachyon model with constant sound speed.

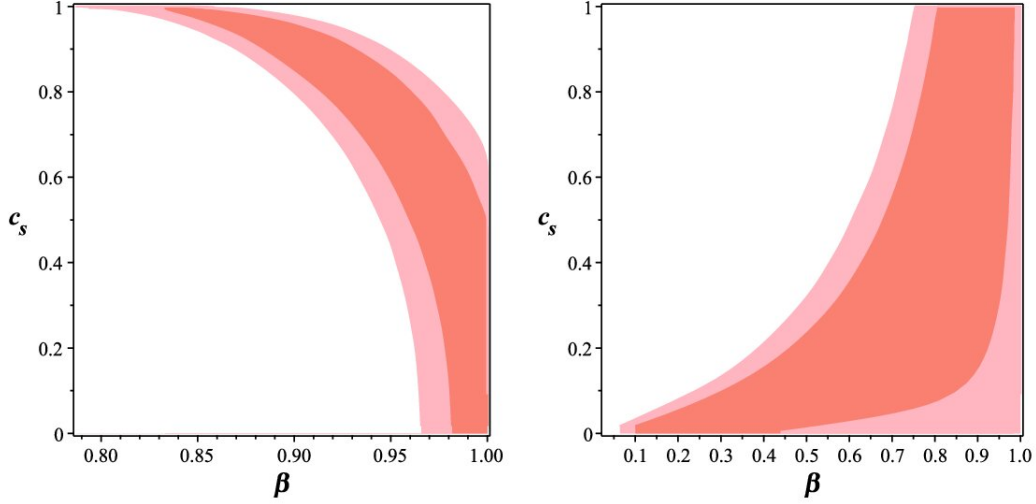


Figure 4: Left panel: ranges of the parameters c_s and β in the intermediate tachyon inflation with constant sound speed, leading to observationally viable values of r versus n_s , obtained from Planck2018 TT, TE, EE+lowE+lensing+BAO+BK14 data at 68% CL (dark region) and 95% CL (light region). Right panel: ranges of the parameters c_s and β in the intermediate tachyon inflation with constant sound speed, leading to observationally viable values of r versus n_T , obtained from Planck2018 TT, TE, EE +lowE+lensing+BK14 +BAO+LIGO and Virgo2016 data at 68% CL (dark region) and 95% CL (light region).

merically and compare the results with observational data. To this end, we consider the amplitudes of the non-gaussianity in equilateral and orthogonal configurations, given by equations (43) and (44). In this way, we plot the behavior of the orthogonal amplitude of the non-gaussianity versus the equilateral amplitude of the non-gaussianity, in the background of Planck2018 TTT, EEE, TTE and EET data. The result is shown in the left panel of figure 6. Our numerical analysis shows that the orthogonal and equilateral amplitudes of the non-gaussianity in the intermediate tachyon model with constant sound speed are consistent with Planck2018 TTT, EEE, TTE and EET data at 68% CL if $0.276 \leq c_s$, at 95% CL if $0.213 \leq c_s$, and at 97% CL if $0.186 \leq c_s$. These ranges of the sound speed lead to the observationally viable values of the tensor-to-scalar ratio too. In the right panel of figure 6, we have plotted the phase space of the tensor-to-scalar ratio and the sound speed squared, based on the domain of the sound speed leading to the observationally viable values of the amplitudes of the non-gaussianity. As the figure shows, the values of the tensor-to-scalar ratio are in the domain consistent with Planck2018 TT, TE, EE+lowE+lensing +BAO+BK14 data. We have summarized the prediction of the model for some sample values of the sound speed in table 1. According to our analysis, it seems that the intermediate tachyon model with constant sound speed is an observationally viable inflation model.

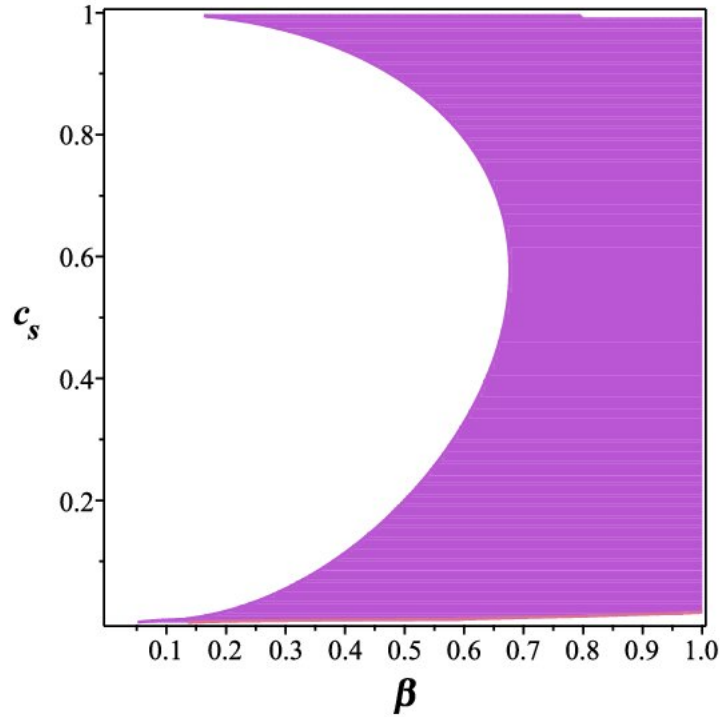


Figure 5: Ranges of the parameters c_s and β in the intermediate tachyon inflation with constant sound speed, leading to observationally viable values of the amplitude of the scalar perturbation.

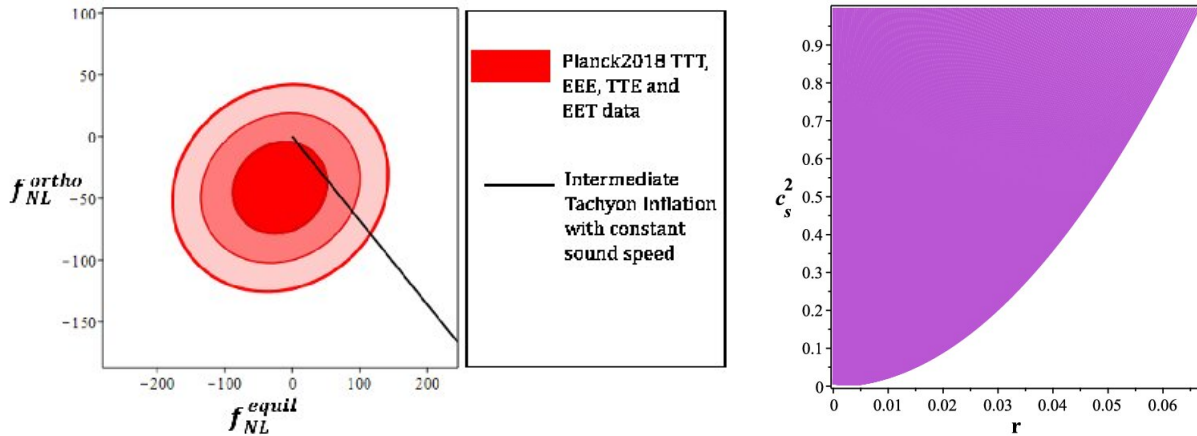


Figure 6: Left panel: orthogonal amplitude of the non-gaussianity versus the equilateral amplitude of the non-gaussianity in the intermediate tachyon model with constant sound speed. Right panel: observationally viable range of the tensor-to-scalar ratio and sound speed squared, based on the observationally viable values of the orthogonal and equilateral amplitudes of the non-gaussianity.

Table 1: Ranges of the parameter β in which the tensor-to-scalar ratio, the scalar spectral index, and the tensor spectral index of the intermediate tachyon model with constant sound speed are consistent with different data sets.

	Planck2018 TT,TE,EE+lowE +lensing+BK14+BAO	Planck2018 TT,TE,EE+lowE +lensing+BK14+BAO	Planck2018 TT,TE,EE+lowE lensing+BK14+BAO +LIGO&Virgo2016	Planck2018 TT,TE,EE+lowE lensing+BK14+BAO LIGO&Virgo2016
c_s	68% CL	95% CL	68% CL	95% CL
0.1	$0.981 < \beta < 1$	$0.965 < \beta < 1$	$0.312 < \beta < 0.859$	$0.250 < \beta < 1$
0.4	$0.968 < \beta < 1$	$0.953 < \beta < 1$	$0.630 < \beta < 0.960$	$0.554 < \beta < 1$
0.7	$0.935 < \beta < 0.970$	$0.920 < \beta < 0.995$	$0.748 < \beta < 0.976$	$0.684 < \beta < 1$
0.9	$0.885 < \beta < 0.931$	$0.871 < \beta < 0.931$	$0.792 < \beta < 0.982$	$0.731 < \beta < 1$

4 Power-Law Tachyon Inflation with Constant-Sound Speed

Now, we study the power-law inflation in the tachyon model with constant sound speed. In the power-law inflation, the scale factor is given by

$$a = a_0 t^n, \quad (50)$$

leading to the following Hubble parameter

$$H(N) = N e^{-\frac{N}{n}}. \quad (51)$$

We use this Hubble parameter and substitute it in equations (47)-(49) to find the inflation parameter in the power-law case. In this way, we can obtain equations (22), (23), (27) and (28) in terms of the model's parameters and perform some numerical analysis on the power-law tachyon inflation with constant sound speed. To obtain some constraints on the model's parameters, we compare the numerical results with observational data. According to our numerical analysis, the power-law tachyon model with constant sound speed is consistent with Planck2018 TT, TE, EE+lowE+lensing+BAO+BK14 data at 95% CL if $0 < c_s \leq 1$ and $222 \leq n \leq 565$. Also, this model is consistent with Planck2018 TT, TE, EE+lowE+lensing+BAO+BK14 data at 68% CL if $0 < c_s < 0.990$ and $293 \leq n \leq 485$. The behavior of the tensor-to-scalar ratio has been shown in figure 7. The running of the scalar spectral index of the power-law tachyon model with constant sound speed versus the scalar spectral index in this model is shown in figure 8. By studying these parameters, we find that in this case, the model is consistent with Planck2018 TT, TE, EE+lowE+lensing data at 68% CL if $0 < c_s \leq 1$ and $299 \leq n \leq 473$ and at 95% CL if $0 < c_s \leq 1$ and $231 \leq n \leq 551$. Figure 9 shows the evolution of the tensor-to-scalar ratio of the power-law tachyon model with constant sound speed versus the tensor spectral index in this model, in the background of the Planck2018 TT, TE, EE +lowE+lensing+BK14 +BAO+LIGO and Virgo2016 data. In this case, the model has observational viability if $0 < c_s \leq 1$ and $27.3 \leq n \leq 3200$ at 68% CL, and $0 < c_s \leq 1$ and $1.67 \leq n$ at 95% CL.

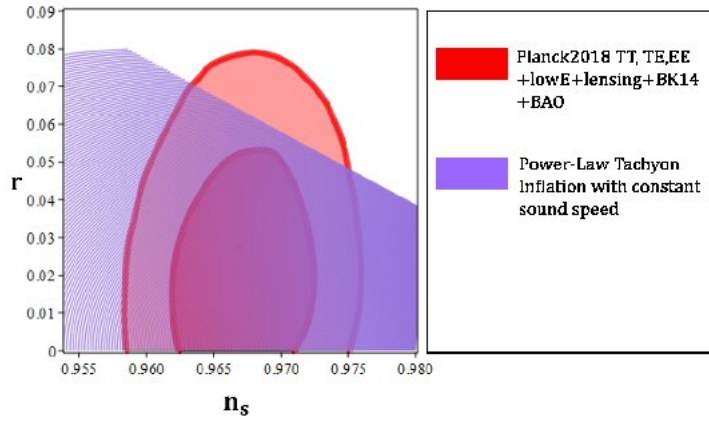


Figure 7: Tensor-to-scalar ratio versus the scalar spectral index in the power-law tachyon model with constant sound speed.

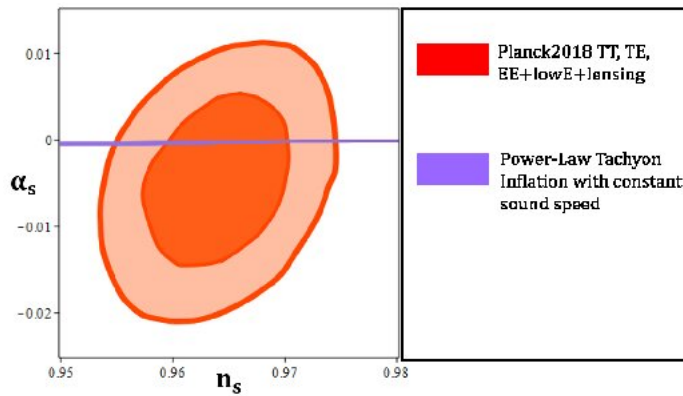


Figure 8: Running of the scalar spectral index versus the scalar spectral index in the power-law tachyon model with constant sound speed.

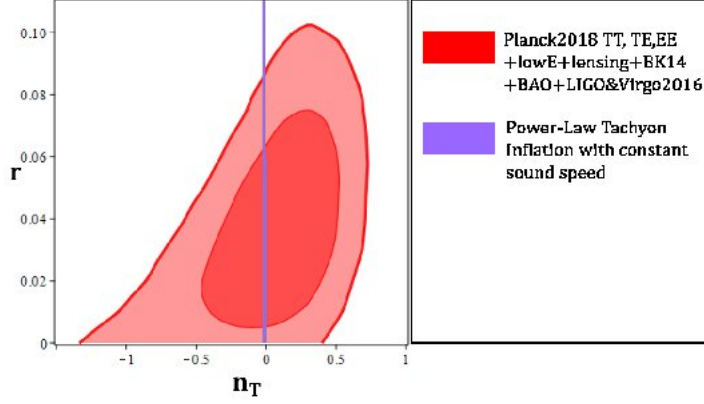


Figure 9: Tensor-to-scalar ratio versus the tensor spectral index in the power-law tachyon model with constant sound speed.

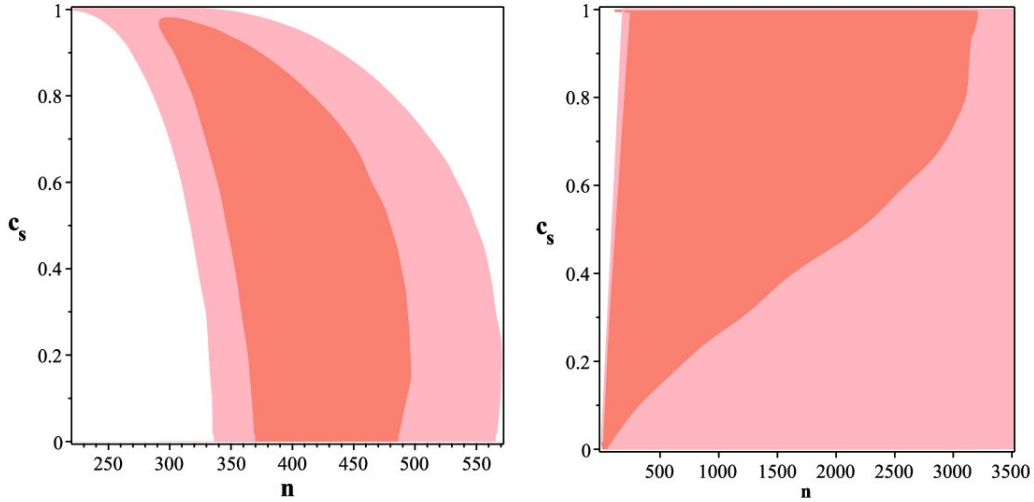


Figure 10: Left panel: ranges of the parameters c_s and n in the power-law tachyon inflation with constant sound speed, leading to observationally viable values of r versus n_s , obtained from Planck2018 TT, TE, EE+lowE+lensing+BAO+BK14 data at 68% CL (dark region) and 95% CL (light region). Right panel: ranges of the parameter c_s and n in the power-law tachyon inflation with constant sound speed, leading to observationally viable values of r versus n_T , obtained from Planck2018 TT, TE, EE +lowE+lensing+BK14 +BAO+LIGO, and Virgo2016 data at 68% CL (dark region) and 95% CL (light region).

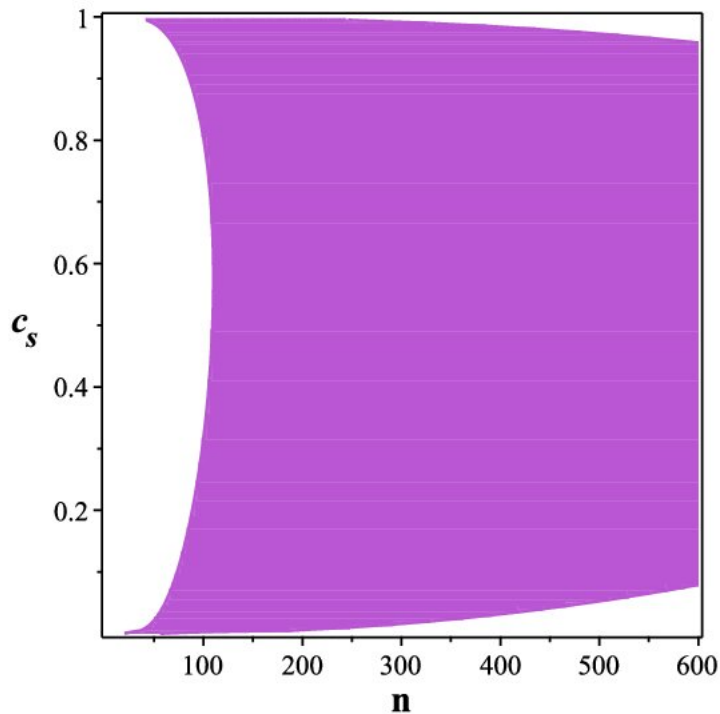


Figure 11: Ranges of parameter c_s and n in the power-law tachyon inflation with constant sound speed, leading to observationally viable values of the amplitude of the scalar perturbation.

Table 2: Ranges of the parameter n in which the tensor-to-scalar ratio, the scalar spectral index, and the tensor spectral index of the power-law tachyon model with constant sound speed are consistent with different data sets.

	Planck2018 TT,TE,EE+lowE +lensing+BK14+BAO	Planck2018 TT,TE,EE+lowE +lensing+BK14+BAO	Planck2018 TT,TE,EE+lowE lensing+BK14+BAO +LIGO&Virgo2016	Planck2018 TT,TE,EE+lowE lensing+BK14+BAO LIGO&Virgo2016
c_s	68% CL	95% CL	68% CL	95% CL
0.1	$368 < n < 492$	$336 < n < 569$	$27.3 < n < 300$	$20.1 < n$
0.4	$354 < n < 488$	$324 < n < 559$	$102 < n < 1600$	$76.0 < n$
0.7	$330 < n < 447$	$301 < n < 511$	$177 < n < 2930$	$131 < n$
0.9	$305 < n < 373$	$270 < n < 483$	$228 < n < 3130$	$167 < n$

The domain of n and c_s , leading to observationally viable values of scalar spectral index, tensor spectral index, and the tensor-to-scalar ratio is shown in figure 10, where we have used both Planck2018 TT, TE, EE+lowE+lensing +BAO+BK14 and Planck2018 TT, TE, EE +lowE+lensing+BK14 +BAO+LIGO and Virgo2016 data sets at 68% CL and 95% CL. It is clear that, although from the observationally viable values of the tensor spectral index we can't find an upper bound on the parameter n , the observational values of the scalar spectral index imply an upper limit on it. These observationally viable ranges of c_s and n lead to the value of the amplitude of the scalar perturbations released by planck2018 data ($\ln(10^{10} A_s) = 3.044 \pm 0.014$). Figure 11 shows this issue clearly. Considering that the sound speed is constant, the behavior of the orthogonal amplitude of the non-gaussianity versus the equilateral amplitude of the non-gaussianity in the power-law tachyon case is the same as the one in the intermediate tachyon case. This means that in this case also we have consistency with Planck2018 TTT, EEE, TTE and EET data at 68% CL if $0.276 \leq c_s$, at 95% CL if $0.213 \leq c_s$, and at 97% CL if $0.186 \leq c_s$. These ranges are compatible with the ranges obtained from n_s , α_s , n_T and r . Therefore, the power-law tachyon inflation with constant sound speed seems to be a fine model that in some ranges of its parameter space is consistent with observational data. In table 2, we have summarized some constraints obtained in studying the power-law tachyon inflation with constant sound speed.

5 A Discussion on Unifying the Inflation with Dark Energy

Currently, cosmologists have been interested in the models covering a larger domain in the thermal history of the universe. In this way, the models that can describe both very early time and very late time accelerating expansion of the universe have attracted a lot of attention. In this respect, in some viable models of $f(R)$ gravity it is possible to describe both early time inflation and late time acceleration of the universe [33, 34, 16, 35]. For instance, in Ref. [34] the authors have considered a model of $f(R)$ gravity where the universe effectively starts with a large cosmological constant at the early universe (leading to inflation) and after passing the radiation/matter dominated era, reaches the small values of the cosmological constant (leading to late time accelerating expansion). In Ref. [35] another model of $f(R)$ gravity that can explain the initial inflation, and at the late time can reproduce the behavior of the Λ CDM model. As we have mentioned in the ‘‘Introduction’’ section, the equation of state of the tachyon field can be -1 , corresponding to late time dark energy and early time inflationary phases of the universe. Therefore, in our model also, it seems possible to unify the inflation with dark energy. As we know, the tachyon inflation with constant sound speed is an observationally viable inflation model, at least in some domains of its parameter space. After inflation ends, and the tachyon field reaches the non-zero minimum of the potential, the universe becomes radiation dominated. During the radiation and matter dominated universe, the minimum value of the potential doesn't disturb the thermal history of the universe. With more expansion of the universe, the energy densities of the radiation and matter become small and eventually at the late time the potential become the dominant component in the energy density of the universe. In fact, this dominant component of the energy density can be considered as an effective cosmological constant, leading to late time accelerating expansion of the universe. It is also possible to consider some extension of the tachyon field so we can get both inflation and late time acceleration in the model. For instance, by considering the non-minimal coupling or non-minimal derivative coupling between the tachyon field and the gravity, depending on the values of the non-minimal parameter,

it may possible to have a model covering both initial inflation and late time acceleration.

6 Conclusion

In this paper, we have considered tachyon inflation where the sound speed is constant. We have obtained the Friedmann equations and equation of motion in terms of sound speed. After that, we have presented the main perturbation parameters, like the scalar spectral index, its running, tensor spectral index, and tensor-to-scalar ratio. We have also, by considering the three-point correlations, presented the amplitude of the non-gaussianity in both equilateral and orthogonal configurations. Then, we have adopted two types of scale factor: Intermediate and power-law. We have studied both cases separately. To study these cases, we have obtained the potential and inflation parameters in terms of the Hubble parameter, its derivative, and also the sound speed. In this way, we were able to study the model based on two types of scale factor. By considering the intermediate scale factor, we have studied $r-n_s$ behavior in the background of Planck2018 TT, TE, EE+lowE+lensing +BAO+BK14 data in both 68% CL and 95% CL and found some constraints on the model's parameters. The behavior of $\alpha_s - n_s$ in the background of Planck2018 TT, TE, EE+lowE+lensing data has been studied too. Another important parameter is the tensor scalar spectral index corresponding to the primordial perturbations. In this way, we have studied $r - n_T$ behavior in the background of Planck2018 TT, TE, EE +lowE+lensing+BK14 +BAO+LIGO and Virgo2016 data to find some constraints on the model's parameter space. We have also analyzed c_s and β phase space in both 68% CL and 95% CL. By studying these parameters numerically, we have found that intermediate tachyon inflation with constant sound speed is observationally viable if $0 < c_s \leq 0.997$ and $0.833 \leq \beta \leq 0.984$ at 68% CL, and $0 < c_s \leq 1$ and $0.787 \leq \beta \leq 1$ at 95% CL. To check the viability of the model more precisely, we have studied the non-gaussian feature of the primordial perturbations. In this regard, we have considered the Planck2018 TTT, EEE, TTE and EET constraints on the equilateral and orthogonal configurations of the non-gaussianity. In this way, we have obtained the constraints on the sound speed as $0.276 \leq c_s \leq 1$ at 68% CL, $0.213 \leq c_s \leq 1$ at 95% CL, and $0.186 \leq c_s \leq 1$ at 97% CL. We have also studied $c_s^2 - r$ phase space and found that the ranges of the sound speed, obtained from the observational constraints on the non-gaussianity, lead to the observationally viable values of the tensor-to-scalar ratio.

The power-law tachyon inflation with constant sound speed is another model that has been studied in this paper. Similar to the intermediate tachyon inflation case, we have studied the perturbation parameters in this model, but here, based on the power-law scale factor. In this case, by using different data sets, we have studied $r-n_s$, $\alpha-n_s$, and $r-n_T$ behavior. The phase space of the parameters c_s and n , based on the observationally viable ranges of the scalar and tensor spectral indices has been studied too. Our numerical analysis has shown that the power-law tachyon inflation with constant sound speed is observationally viable for $0 < c_s \leq 0.990$ and $299 \leq n < 473$ at 68% CL, and $0 < c_s \leq 1$ and $231 \leq n < 551$ at 95% CL. For these obtained ranges, the amplitude of the scalar spectral index is consistent with observational data. We have also discussed the issue of unifying the inflation with dark energy in the tachyon model with constant sound speed. We have argued that the non-zero minimum value of the tachyon potential becomes important at the late time, after the energy density of the radiation/matter decreases. Based on our analysis, it seems that both intermediate and power-law tachyon models in some ranges of their parameter space are consistent with observational data.

Acknowledgement

I thank the referee for the very insightful comments that have improved the quality of the paper considerably.

References

- [1] Ade, P. A. R. , Aghanim, N., Arnaud, M., et al. *Astron. Astrophys.*, 2016, **594**, A20
- [2] Aghanim, N., Akrami, Y., Ashdown, M., et al. 2018, arXiv:1807.06209
- [3] Akrami, Y., Arroja, F., Ashdown, M., et al. 2018, arXiv:1807.06211
- [4] Akrami, Y., Arroja, F., Ashdown, M., et al. 2019, arXiv:1905.05697
- [5] Albrecht, A., & Steinhard, P. 1982, *PhRvD*, **48**, 1220
- [6] Babich, D., Creminelli, P., & Zaldarriaga, M. 2004, *JCAP*, **0408**, 09
- [7] Bamba, K., Nojiri, S., Odintsov, S. D., & Gomez, D. S. 2014, *PhRvD*, **90**, 124061
- [8] Barrow, J. D. 1990, *Physics Letters B*, **235**, 40
- [9] Barrow, J. D., & Liddle, A. R. 1993, *PhRvD*, **47**, 5219
- [10] Barrow, J. D., & Nunes, N. J. 2007, *PhRvD*, **76**, 043501
- [11] Baumann, D. 2012, arXiv:0907.5424
- [12] Bilic, N. Dimitrijevic, D. D., Djordjevic, G. S., Milosevic, M., & Stojanovic, M. 2019, *JCAP*, **08**, 034
- [13] Bouabdallaoui, Z., Errahmani, A., Bouhmadi-López, M., & Ouali, T. 2016, *PhRvD*, **94**, 123508
- [14] Byrnes, C. T. 2014, arXiv:1411.7002
- [15] Chen, X., Huang, M. -X., Kachru, S., & Shiu, G. 2007, *JCAP*, **0701**, 002
- [16] Cognola, G., Elizalde, E., Nojiri, S., Odintsov, S. D., Sebastiani, L., & Zerbini, S., 2008, *PhRvD*, **77**, 046009
- [17] De Felice, A., & Tsujikawa, S. 2011, *JCAP*, **03**, 030
- [18] Fergusson, J. R., & Shellard, E. P. S. 2009, *PhRvD*, **80**, 043510
- [19] Gibbons, G.W. 2002, *Phys. Lett. B*, **537**, 1
- [20] Guth, A. 1981, *PhRvD*, **23**, 347
- [21] Hu, W., Seljak, U., White, M., & Zaldarriaga, M. 1998, *PhRvD*, **57**, 3290

- [22] Hu, W., & White, M. J. 1997, *PhRvD*, **56**, 596
- [23] Kamali, V., Basilakos, S., Mehrabi, A., Motaharfar, M., & Massaelli, E. 2018, *International Journal of Modern Physics D*, **27**, 1850056
- [24] Kamionkowski, M., Kosowsky, A., Stebbins, A., et al. 1997, *PhRvD*, **55**, 7368
- [25] Liddle, A., & Lyth, D. 2000, *Cosmological Inflation and Large-Scale Structure* (Cambridge University Press)
- [26] Lidsey, J. E., Liddle, A. R., Kolb, E. W., Copeland, E. J., Barreiro, T., & Abney, M. 1997, *Abney, Rev. Mod. Phys.*, **69**, 373
- [27] Linde, A. D. 1982, *Phys. Lett. B*, **108**, 389
- [28] Linde, A. D. 1990, *Particle Physics and Inflationary Cosmology* (Harwood Academic Publishers, Chur, Switzerland)
- [29] Lyth, D. H., & Liddle, A. R. 2009, *The Primordial Density Perturbation* (Cambridge University Press)
- [30] Maldacena, J. M. 2003, *JHEP*, **0305**, 013
- [31] Mohammadi, A., Golanbari, T., Sheikahmadi, H., Sayar, K., Akhtari, L., Rasheed, M. A., & Saaidi, K. 2020, *Chinese Phys. C*, **44**, 095101
- [32] Nojiri, S., & Odintsov, S. D. 2003, *Phys. Lett. B*, **571**, 1-10
- [33] Nojiri, S., & Odintsov, S. D. 2007, *PhLB*, **657**, 238
- [34] Nojiri, S., & Odintsov, S. D. 2008, *PhRvD*, **77**, 026007
- [35] Nojiri, S., & Odintsov, S. D. 2011, *Phys. Rept.*, **505**, 59-144
- [36] Nozari, K., & Rashidi, N. 2014, *PhRvD*, **88**, 023519
- [37] Odintsov, S.D., & Oikonomou, V.K. 2015, *Ann. Phys.* **363**
- [38] Rashidi, N. 2021, *The Astrophysical Journal*, **914**, 29
- [39] Rashidi, N., & Nozari, K. 2018, *IJMPD* **27**, 1850076
- [40] Rashidi, N., & Nozari, K. 2020, *The Astrophysical Journal*, **890**, 55
- [41] Rezazadeh, K., Karami, K., & Hashemi, S. 2017, *PhRvD*, **95**, 103506
- [42] Riotto, A. 2002, *arXiv:hep-ph/0210162*
- [43] Seljak, U., & Zaldarriaga, M. 1997, *Phys. Rev. Lett.* **78**, 2054
- [44] Sen, A. 1999, *JHEP*, **10**, 008
- [45] Sen, A. 2002, *JHEP*, **07**, 065

- [46] Sen, A. 2002, *MPLA*, **17**, 1797
- [47] Spalinski, M. 2007, *JCAP*, 0705, 017
- [48] Tsujikawa, S., Ohashi, J., Kuroyanagi, S., & De Felice, A. 2013, *PhRvD*, **88**, 023529
- [49] Zaldarriaga, M., & U. Seljak, U. 1997, *PhRvD*, **55**, 1830